

# Energy Dissipation of Liquids in Nutating Spherical Tanks Measured by a Forced Motion-Spin Table

MICHAEL F. ZEDD

*Mechanical Systems Branch  
Space Systems and Technology Division*

AND

FRANKLIN T. DODGE

*Department of Mechanical Sciences  
Southwest Research Institute  
San Antonio, Texas*

October 30, 1985



**NAVAL RESEARCH LABORATORY**  
Washington, D.C.

SECURITY CLASSIFICATION OF THIS PAGE

<b>REPORT DOCUMENTATION PAGE</b>				
1a. REPORT SECURITY CLASSIFICATION <b>UNCLASSIFIED</b>		1b. RESTRICTIVE MARKINGS		
2a. SECURITY CLASSIFICATION AUTHORITY		3. DISTRIBUTION / AVAILABILITY OF REPORT		
2b. DECLASSIFICATION / DOWNGRADING SCHEDULE		Approved for public release; distribution unlimited.		
4. PERFORMING ORGANIZATION REPORT NUMBER(S)  NRL Report 8932		5. MONITORING ORGANIZATION REPORT NUMBER(S)		
6a. NAME OF PERFORMING ORGANIZATION  Naval Research Laboratory	6b. OFFICE SYMBOL (if applicable)  Code 7730	7a. NAME OF MONITORING ORGANIZATION		
6c. ADDRESS (City, State, and ZIP Code)  Washington, DC 20375-5000		7b. ADDRESS (City, State, and ZIP Code)		
8a. NAME OF FUNDING / SPONSORING ORGANIZATION	8b. OFFICE SYMBOL (if applicable)	9. PROCUREMENT INSTRUMENT IDENTIFICATION NUMBER		
8c. ADDRESS (City, State, and ZIP Code)		10. SOURCE OF FUNDING NUMBERS		
		PROGRAM ELEMENT NO. 30000 N	PROJECT NO.	TASK NO.
				WORK UNIT ACCESSION NO. EX080-165
11. TITLE (Include Security Classification)  Energy Dissipation of Liquids in Nutating Spherical Tanks Measured by a Forced Motion-Spin Table				
12. PERSONAL AUTHOR(S) Zedd, Michael F., and Dodge, Franklin T.				
13a. TYPE OF REPORT Final	13b. TIME COVERED FROM 7/82 TO 7/84	14. DATE OF REPORT (Year, Month, Day) 1985 October 30	15. PAGE COUNT 24	
16. SUPPLEMENTARY NOTATION				
17. COSATI CODES			18. SUBJECT TERMS (Continue on reverse if necessary and identify by block number)	
FIELD	GROUP	SUB-GROUP		
			Sloshing waves Spin Mechanical model	
			Inertial waves Nutation Spherical tanks	
			Liquid resonances Energy dissipation Prolate-spinning-spacecraft	
19. ABSTRACT (Continue on reverse if necessary and identify by block number)				
<p>A specially constructed drive table is described that can spin and nutate scale-model propellant tanks. Results of typical tests are given in which the liquid resonant frequencies and liquid forces and moments are presented as a function of spin rate, nutation frequency, nutation cone angle, liquid filling level, and liquid viscosity. Also described is an empirical mechanical model composed of a pendulum, a rotor, and dashpots that simulate the liquid resonances (slosh and inertial waves) and the liquid forces and moments. The parameters of the model are determined from the propellant motions.</p>				
20. DISTRIBUTION / AVAILABILITY OF ABSTRACT <input type="checkbox"/> UNCLASSIFIED/UNLIMITED <input checked="" type="checkbox"/> SAME AS RPT. <input type="checkbox"/> DTIC USERS			21. ABSTRACT SECURITY CLASSIFICATION <b>UNCLASSIFIED</b>	
22a. NAME OF RESPONSIBLE INDIVIDUAL Michael F. Zedd		22b. TELEPHONE (Include Area Code) (202) 767-1747	22c. OFFICE SYMBOL Code 7735	

DD FORM 1473, 84 MAR

83 APR edition may be used until exhausted.  
All other editions are obsolete.

SECURITY CLASSIFICATION OF THIS PAGE

## CONTENTS

DEFINITIONS .....	v
INTRODUCTION .....	1
QUALITATIVE LIQUID MODE DESCRIPTIONS .....	2
MECHANICAL MODEL .....	3
FORCED MOTION-SPIN TABLE .....	3
Model Tank Construction and Instrumentation .....	8
Phase-Angle Determination .....	9
TEST PLAN .....	9
EXPERIMENTAL RESULTS .....	10
Calibration .....	10
Determining Model Parameters .....	11
SCALING RELATIONS .....	13
SUMMARY .....	13
ACKNOWLEDGMENTS .....	14
REFERENCES .....	14
APPENDIX — Analysis of Models .....	15

## DEFINITIONS

$d$	tank diameter
$e_x, e_y$	empirical parameters to skew the boundary layer on a rotating sphere
$g$	acceleration of gravity
$k_x, k_y$	empirical parameters to model "free stream" velocity at wall
$l_s$	slosh pendulum length
$t$	time
$x, y, z$	tank fixed coordinate system
$C(C_x, C_y)$	dashpot representing boundary layer viscous shear about $x, y$ axes, respectively
$C_s$	dashpot representing viscous damping of slosh modes
$D(D_x, D_y)$	dashpot representing viscous damping of inertial wave modes along $x, y$ axes, respectively
$E_I, E_s$	energy dissipation rate, per nutation cycle, for inertial and sloshing oscillations
$F(F_x, F_y, F_z)$	oscillating liquid force exerted on tank and its force components along $x, y, z$ axes, respectively
$I_x, I_y, I_z$	moments of inertia of rotor
$M(M_x, M_y, M_z)$	oscillating liquid moment exerted on tank and its moment components about $x, y, z$ axes, respectively
$M_0, M_s$	nonslosh and slosh liquid masses
$M_T$	total liquid mass = $M_0 + M_s$
$T_x, T_y$	moments exerted on tank wall by viscous boundary layer
$X_0, Z_0$	location of tank center
% Full	tank filling percentage
$I_s/I_t$	moment of inertia ratio = spin axis/transverse axis moments of inertia

$\alpha, \psi$	angular displacement of pendulum with complex amplitudes $\alpha_0$ and $\psi_0$
$\alpha_y$	tank angular acceleration about $y$ axis
$\gamma_0$	equilibrium angular position of pendulum
$\eta_x, \eta_y$	angular displacements of rotor
$\theta$	cone or nutation half-angle
$\lambda$	nutation frequency or rate
$\mu_\alpha, \mu_\psi$	characteristic frequencies, See Eq. (A4)
$\nu$	kinematic viscosity
$\rho$	liquid density
$\omega_x, \omega_y$	tank rotation rates about $x, y$ axes, respectively
$\Omega$	steady spin rate about $Z$ axis

# ENERGY DISSIPATION OF LIQUIDS IN NUTATING SPHERICAL TANKS MEASURED BY A FORCED MOTION-SPIN TABLE

## INTRODUCTION

A successful spacecraft design — spin stabilized about the axis of minimum moment of inertia and having a large liquid propellant mass fraction — depends on long term vehicle control. Liquid motion in a nutating spacecraft results in kinetic energy dissipation that increases coning motion in the prolate spinner. This coning motion, if not controlled, results in a flat spin, or spin about the axis of maximum moment of inertia. Coning motion must be minimized by active nutation control to maintain the original attitude. Consequently, the maximum energy dissipation rates from the propellant motions must be known to size and to compensate an active nutation control system for these losses.

This report describes an experiment and results of an energy dissipation study of liquid motion using a forced motion spin table. Specifically, this work considers nutating, smooth-walled spherical propellant tanks, without propellant management devices, which spin off center. Energy dissipation rates are estimated by the results of tests having the following objectives:

- identify all liquid resonant frequencies, and spin and nutation conditions under which resonances occur;
- measure oscillating liquid forces and moments as a function of spin rate, nutation rate, coning angle, and liquid fill level;
- determine boundary layer shear at the tank walls; and
- observe and quantify liquid phenomena that might adversely affect prolate spacecraft under the control of spin stabilization.

This research also devises a mechanical model composed of a pendulum, a rotor, and viscous dashpots that can (a) simulate liquid forces and moments, (b) predict liquid resonances and energy dissipation rates, and (c) be used to scale-up test results to flight conditions including gravity field compensation. The numerical values for the model parameters come from the forced motion tests. An equivalent mechanical model of propellant motion is also a practical tool in conducting simulation studies because it can be readily incorporated in spacecraft attitude control models.

The test matrix investigated a wide range of variables. These include:

- spin rate,
- nutation rate or excitation frequency,
- nutation or cone angle,
- fill fraction or percent of tank occupied by liquid,
- liquid density and viscosity, and
- tank location with respect to center of spin.

Although the vehicle inertia ratio is not included as a test parameter, the effective inertia ratio is fixed by the spin rate and nutation rate. The tests actually investigated a wide range of inertia ratios.

## QUALITATIVE LIQUID MODE DESCRIPTIONS

A complete theory of the kinds of motion that can occur in a spinning spherical tank is not available, but the differential equations of motion suggest that two kinds of natural oscillations are possible [1,2]. They are:

- sloshing waves (free surface oscillations), and
- inertial waves (internal liquid oscillations).

In general, both kinds of waves produce oscillating forces and moments about the center of an arbitrary shaped tank. But for a spherical tank, liquid pressure can create only a force; thus any moment exerted about the tank center can only be due to viscous shear at the wall. Ordinarily, viscous shear is negligible compared to the effects of pressure [3]. Similarly, an oscillating rotation of a spherical tank about its own center is transmitted to the liquid only by viscous shear at the wall. For other tank shapes, viscous shear is ineffective compared to the oscillating wall motion normal to the wall surfaces. One of the items of interest is to determine if viscous shear could cause significant inertial waves in a spinning spherical tank. The following discussion of liquid motion is described from the point of view of a coordinate system fixed to the tank center. In this system, nutation causes oscillatory translations along all three axes and oscillatory rotations about the two axes that lie in the plane normal to the spin axis.

*Sloshing waves* are characterized by oscillations of the free surface and center of mass location such as to change the potential energy of the liquid relative to the effective gravity force. The effective gravity is a vector combination of the true gravity and centripetal accelerations. Sloshing is a dynamic interaction between effective gravity forces and inertial forces. There must be a free surface and it must move up and down through the gravity field. Mathematically, sloshing can be analyzed on the basis of an ideal liquid executing an irrotational motion, that is, as potential flow. The effects of viscosity may be considered later as a boundary layer at the wall; the effect is to provide some damping of the motion, but viscosity does not significantly change the slosh modal characteristics or the natural frequencies. When one of the lower frequency modes is driven at resonance, the damping of an ordinary low viscosity liquid is so small that the wave becomes unstable. For an axisymmetric tank, the instability causes the free surface wave to rotate around the symmetry axis but the bulk of the liquid still has an irrotational potential type of motion. A sloshing wave is primarily excited by unsteady tank translation—not rotation—in a spherical tank.

When the tank spins, the liquid spins with it after some initial transient motion. The liquid motion is thus rotational, and a conventional analysis would not apply. There are some indications that a potential flow-like-sloshing can exist in this rotational field and that all the slosh resonant frequencies are greater than twice the spin rate. Assuming that sloshing can be created in a spinning tank, sloshing resonances can be excited only if the excitation frequency,  $\lambda$ , is more than twice the spin rate.

*Inertial waves* do not require a free surface and can occur in a completely full tank [2]. The center of mass oscillations are small even if the free surface oscillates. The resonances represent a dynamic interaction between Coriolis forces and pressure forces in the bulk of the liquid interior. Inertial waves are circulatory or to-and-fro motions in the liquid interior, and there may or may not be any apparent motions at the free surface. They are excited by unsteady tank rotations. Inertial wave resonant frequencies, regardless of tank shape, are less than twice the spin rate,  $\Omega$  [4,5].

*Boundary layer shear* is the coupling of liquid motion to tank walls via the viscous liquid itself. This is an energy transfer mechanism, and the greater viscosity liquids induce both greater shear and energy dissipation rates. Although the boundary layer is a source of damping, it may drive an inertial wave to resonance in a spherical tank in addition to driving bulk motions.

## MECHANICAL MODEL

To help understand the test results and data analysis described later, the equivalent mechanical model proposed for a spinning spherical tank is described below.

Figure 1 shows an equivalent mechanical model based on the liquid motion characteristics previously described. A pendulum is proposed to represent the predominant mode of sloshing, and a spinning rotor is proposed to represent the predominant mode of inertial oscillations. (Additional pendulums and rotors could be used to represent additional modes of each kind if necessary.) For sloshing, the primary effect of the steady spinning is expected to be the body forces created by the centripetal acceleration. Since this body force effect is similar to that induced either by a steady engine thrust or by gravity, the pendulum model is similar in form to that for a nonspinning spherical tank in a gravity field. The oscillations of the pendulum mass simulate the oscillations of the liquid center of mass. In a spinning tank, however, the pendulum has two natural frequencies, which correspond to oscillations in the circumferential direction and in the transverse direction. For inertial wave oscillations, the steady spinning is crucial since such oscillations do not occur in a nonspinning tank [2]. Thus the equivalent mechanical element must also spin, that is, it should be in the form of a rotor.

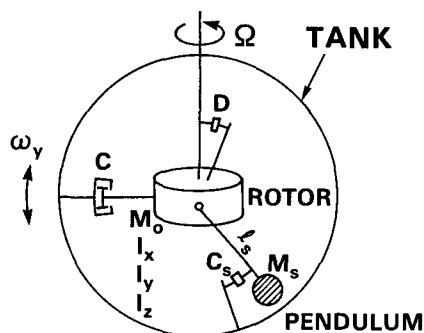


Fig. 1 — Proposed mechanical model

The natural frequency of the rotor is chosen by proper selection of the inertias  $I_x$ ,  $I_y$ , and  $I_z$  to duplicate the natural frequency of the inertial oscillation mode of interest. A rotational viscous dashpot connects the rotor to the tank to simulate the indirect excitation of the liquid caused by viscous shear. The moment exerted on the rotor by the dashpot is not, however, a simple angular rate dependency since it must simulate an unsteady Ekman boundary layer. (Details are given in the appendix of this report.)

## FORCED MOTION-SPIN TABLE

The test stand simulates bodies whose motions can be described by the equations for rotation about a point. Rigid body motion about a fixed point occurs when a symmetrical rotor spins about its axis which itself rotates about a fixed point. Three angles, known as *Euler's angles*, completely specify the position of the rotor. The time rates of change of these angles specify the nutation, precession, and spin velocities of the rotor. The forced motion-spin table simulates this rigid body motion, about a fixed point, with spin rates driven by the outer table, cone angle provided by the gimbal axle, and nutation rates driven by the inner table. Figure 2 shows construction details of the test stand. Figure 3 highlights tank motions and defines symbols.

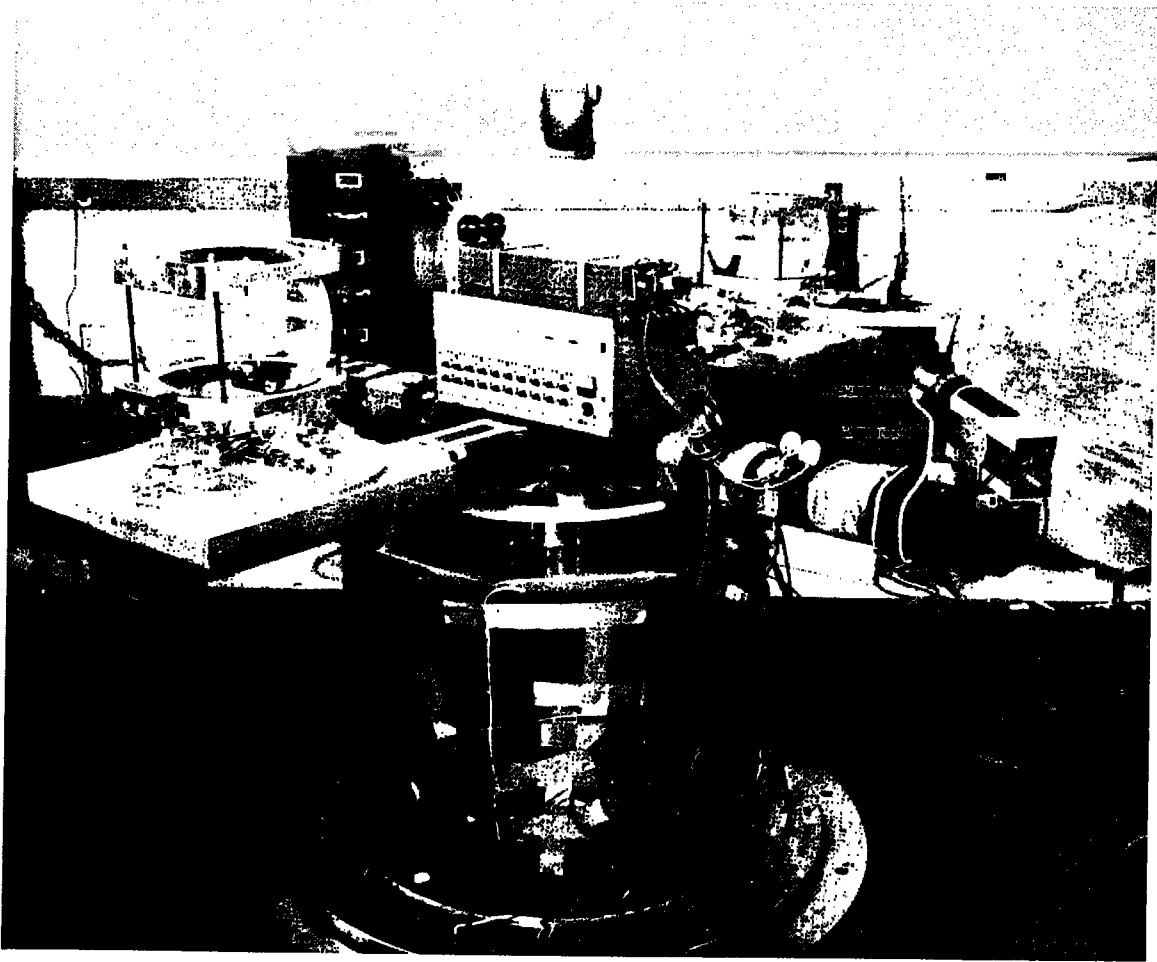


Fig. 2(a) — Construction details of forced motion-spin table

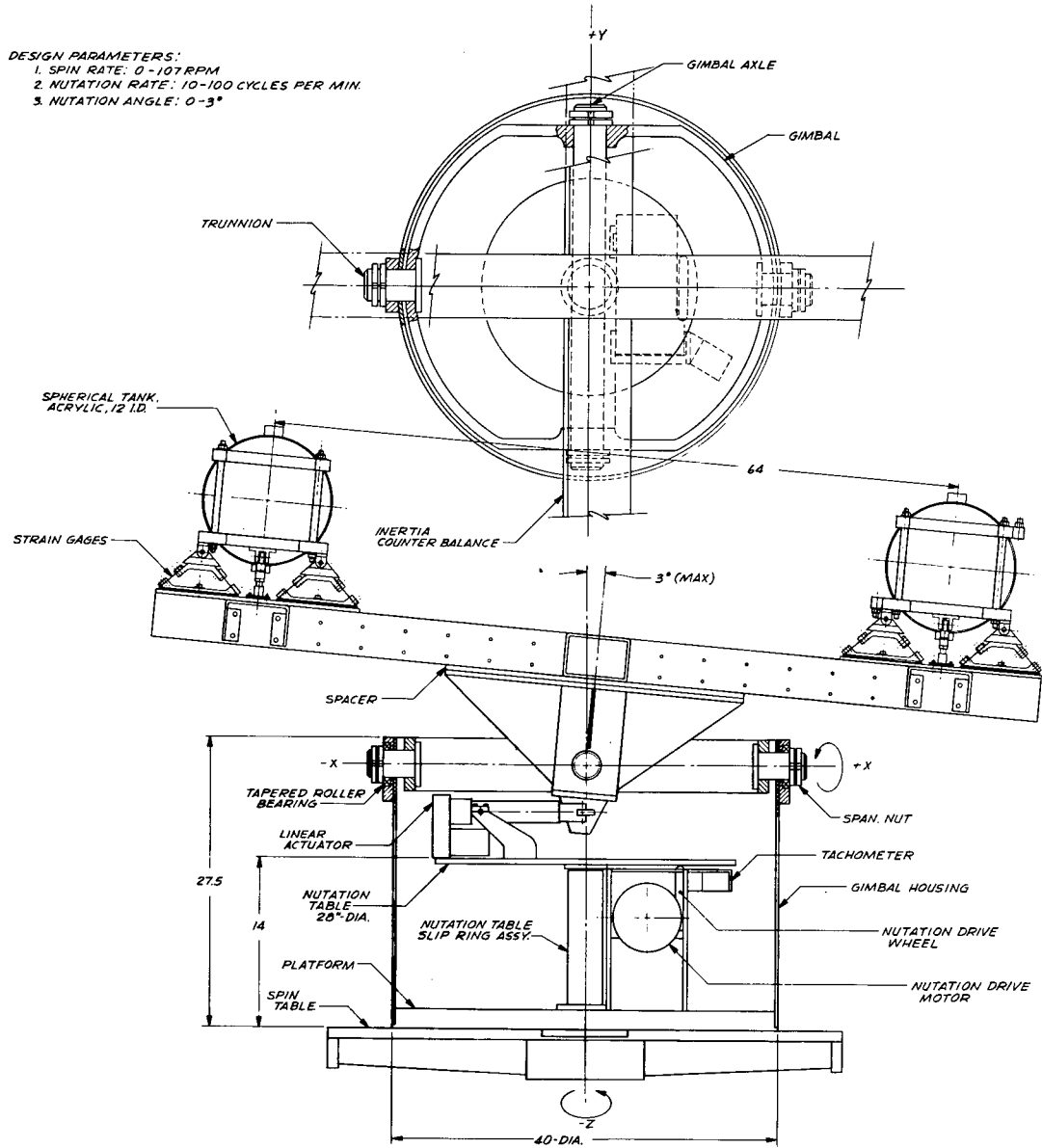


Fig. 2(b) — Construction details of forced motion-spin table

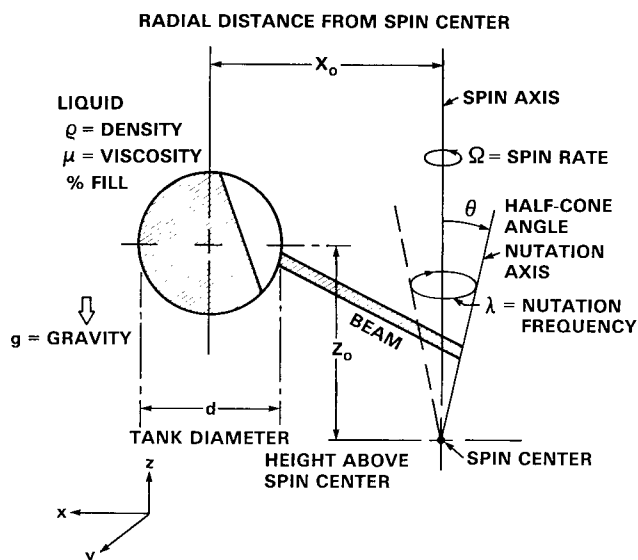


Fig. 3 — Symbols defining spin and tank parameters

The gimbal housing is mounted on top a spin balance table. Below the table are twenty pairs of slip rings used to transfer power to and data from the instrumentation. During a test, the gimbal housing, or outer table, spins about the vertical axis at a constant rate. The housing's most important functions are the support of the gimbal, gimbal axles, and overall fixture weight.

The nutation drive wheel rotates the nutation, or inner, table at speeds different from the outer table. Inner table spin direction is counter to the outer table spin direction when simulating the inertia ratios of prolate spinners.

The lower end of the beam support cone comes to a point that attaches to a linear actuator or piston-in-cylinder mechanism. The piston remains fixed relative to the cylinder to maintain constant nutation, or cone angle. That is, the piston pulls the lower end of the beam support off center and holds this position. The cylinder base, in turn, spins with the nutation table generating constant cone angle.

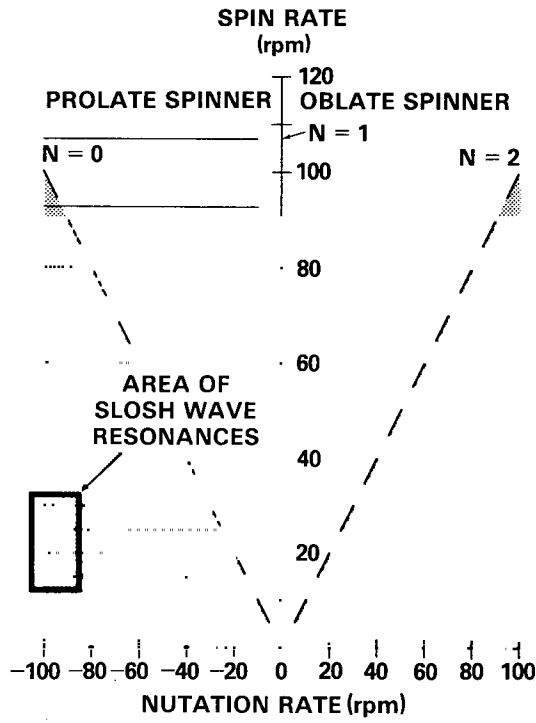
The center of the gimbal axle is the fixed point center of spin. From this point, radial arm length and vertical height to the geometric centers of each tank are measured. Tanks can be relocated along the beam length to vary the radial distance and on top or below the beam to vary the height distance.

An analysis of the rigid body motion produced with this forced motion spin table shows, for small cone angles, the following relationship between spin rate,  $\Omega$ , and nutation rate,  $\lambda$ :

$$\lambda = -(1 - I_s/I_t)\Omega, \quad (1)$$

hence to simulate a prolate spinner where  $I_s/I_t < 1$ ,  $\lambda$  must be of opposite sense as  $\Omega$  with a magnitude given by the above equation. For example, if  $I_s/I_t = 0.50$  and  $\Omega = 60$  rpm (clockwise), then  $\lambda = 30$  rpm (counter-clockwise). Figure 4 shows table operating nutation speeds that correspond to specific inertia ratios. Note the eight horizontal lines representing tests of constant spin rate and counter nutation rates.

SHOWING SLOSH WAVE RESONANCES  
EXCITED OUTSIDE PHYSICALLY  
REALIZABLE INERTIA RATIOS



TEST RUN AT CONSTANT SPIN RATE  
AS NUTATION RATE INCREASED  
FROM 10 TO 100 RPM COUNTER TO  
SPIN DIRECTION

$$N = \frac{I_{SPIN}}{I_{TRANSVERSE}}$$

$$\lambda = (N - 1)\Omega$$

Fig. 4 — Forced motion-spin table operating regions

### Model Tank Construction and Instrumentation

Forces and moments imparted to the tank by liquid motions are the fundamental quantities to be measured from this experiment. This section reviews propellant tank model instrumentation used to accomplish this objective. The liquid tank and an equivalent weighted control tank are each supported by a strain-gage-dynamometer assembly. Figure 5 identifies the tank mount components and defines the tank centered coordinate system.

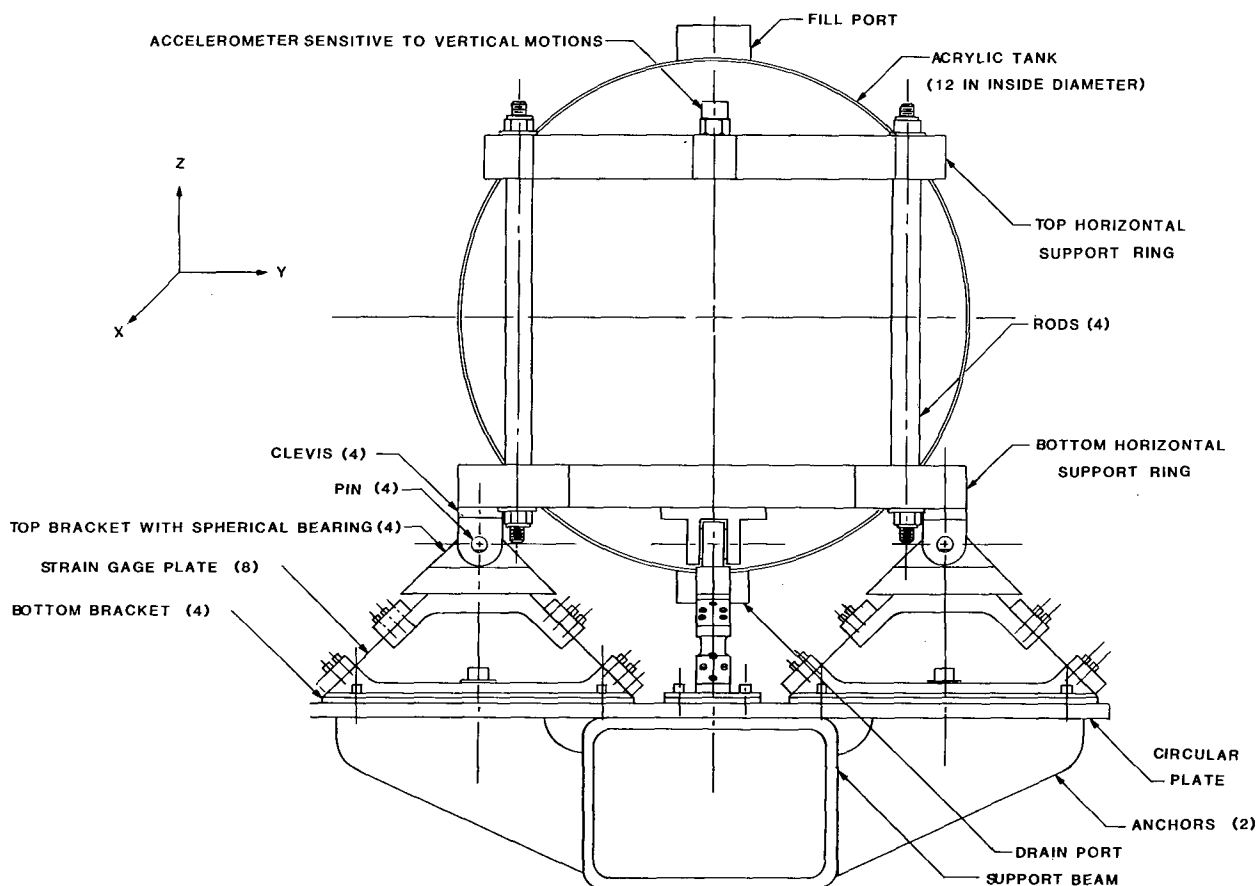


Fig. 5 — Tank component identification

The plastic tank is held between two support rings by four rods bolted through the corners of each ring. These rods compress the rings around the tank. The plastic has been slightly deformed from spherical shape reacting to the compression necessary to hold it rigid.

A clevis attaches underneath each side of the horizontal support ring. The top bracket is solid and holds a spherical bearing previously pressed-fit into its side. This bearing fits into the clevis, and a pin is friction-fit through both clevis and bearing. Washers, used as spacers, prevent further sliding. The top bracket clamps to each of two strain-gage-plates, which in turn clamp to the bottom bracket. Finally, the four bottom brackets bolt on a circular plate that anchors to the beam.

The dynamometers, each pair responding to forces along one axis, are the components between the pin and the circular plate. The reaction end of the dynamometers is pinned through the spherical

bearing to prevent the introduction of end moments into the dynamometer. Ideally, only unidirectional forces act on the dynamometer, thus achieving pure tension or compression on the sections.

The gaging sections of the strain-gage plates are only long enough to accommodate the strain gages placed on them. The remainder of the dynamometer is as rigid as possible. This combination results in the highest possible buckling strength and stiffness. The system is not responsive to moments about the  $z$ -axis; but all other forces ( $F_x, F_y, F_z$ ) and moments ( $M_x, M_y$ ) are resolved. Five strain-gage bridges per tank sample the three axis forces and two moment components produced by the liquid reaction to externally forced tank motions. Linear accelerometers mount on the liquid tank to provide reference motion for calculation of liquid phase lag. The recorded force, moment, and phase lag magnitudes vs the nutation frequency of excitation provide the basis for dissipation rate calculations. These recordings along with qualitative descriptions of liquid motions, observed via video camera mounted on the cross beam, complete the output data base.

Ten strain gage conditioners power ten bridges and continuously sample signal out from them. These conditioners and two accelerometer charge amplifiers are located at the center of the crossed beams. Line power to these conditioners and amplifiers, and output data from them transfer through slip rings.

The ten data channels pass into ten separate filtering circuits that rectify and eliminate the dc bias. The dc bias is the steady component of total signal representing the centripetal force along  $F_x$  and  $M_y$ . The ac component of the original signal is the desired sample. An ac filter attenuates the noise signals above 4 Hz. The rms-to-dc chip takes the absolute value of this signal, multiplies it by 0.707, then converts it to a dc result representing the rms value.

### Phase Angle Determination

Two accelerometers provide the tank motion reference; linear and angular motions are sensed. One accelerometer is mounted on the top horizontal ring, outboard side, and the other, on the bottom horizontal ring, inboard side. The positive axes of both accelerometers are mounted along the vertical in opposite directions. Subtraction of linear components result in a reference signal proportional to the angular acceleration,  $\alpha_y$ , about the  $y$ -axis. The phase of the  $M_y$  signal relative to the  $\alpha_y$  signal was then determined by electronically measuring the time difference between the peaks of the two signals. In practice, the  $M_y$  gage system senses the moment of all forces and couples above the spherical bearings (Fig. 5). Thus the desired signal proportional to the viscous shear couple about the tank center was not measured directly, which somewhat diminished the usefulness of the phase-angle measurements as a method of estimating energy dissipation rates.

### TEST PLAN

Tests represented conditions with water or glycerol as the sloshing liquid in tanks located at 32 in. radius and 21 or 22 in. above spin center. The lower support ring of the control tank was weighted with lead equal to liquid weight. Beginning with the desired fill fraction (50, 75, or 100%) and nutation angle (1°, 2°, or 3°), a constant outer table spin rate (0, 15, 20, 25, 30, 60, 80, 92.5, 107 rpm) was selected. The nutation (inner) table was rotated from 10 to 100 rpm and at 2-rpm intervals, the sensors were sampled. Each nutation frequency was held constant for a time sufficient to allow transients to decay. Data were plotted by computer after completing a test. This readily showed a liquid slosh resonance in which the increased force and moment observed in the liquid tank was not seen in the control. Not every test condition produced one of these resonances. Another test condition was selected and the test repeated. All results were used for boundary layer shear computations.

Fifteen of the 81 tests with water were repeated with glycerol solution (with viscosity ten times greater than water) to verify selected model damping parameters.

## EXPERIMENTAL RESULTS

Figure 6 shows a typical slosh-wave resonance excited at a low spin rate and high nutation rate. Here,  $F_y$  exhibits the classic resonance response. We note that its moment pair,  $M_x$ , showed similar shape. The  $F_x$  and  $M_y$  pair were mirror images of these; their magnitudes decreased before sharply rising. This was affected by rotation of the nodal line of the surface wave around the tank.

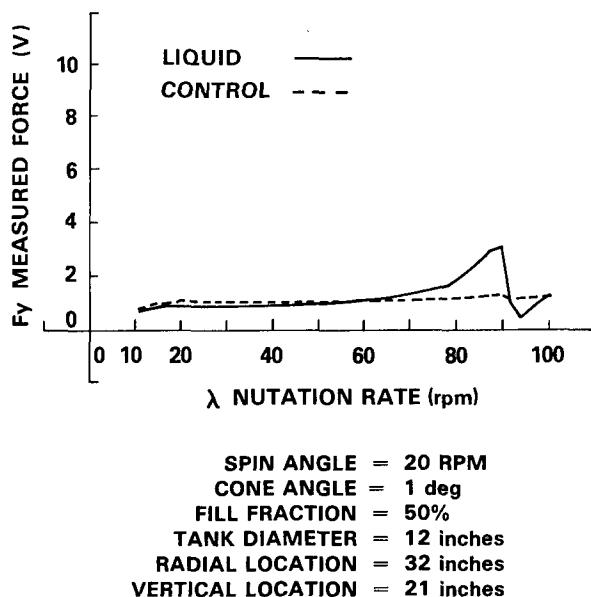


Fig. 6 — Typical low spin-speed result showing slosh-wave resonance

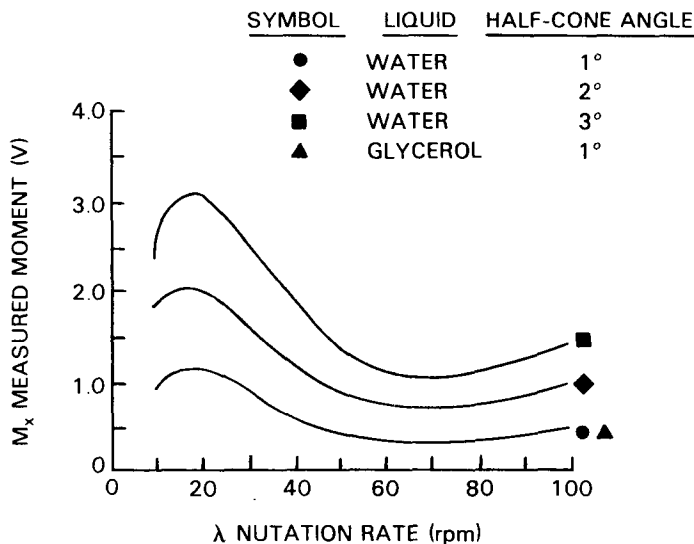
Figure 7 shows responses excited at high spin rate and low nutation rate. All high spin rates ( $\Omega \geq 60$  rpm) excited a structural resonance in the table. Note increasing amplitude as a function of  $\theta$  and that changing viscosity does not greatly affect amplitude.

### Calibration

Voltage outputs of the strain gages were calibrated by using different methods, depending upon table resonance.

The table did not resonate at low spin rate ( $\Omega \leq 30$  rpm). In this spin region, the dynamic calibration method required determining the expected forces and moments sensed by the dynamometers according to the principles of dynamics, for nutation frequencies well below the slosh resonances. Calibration curves resulted from loading the empty liquid tank's lower horizontal ring with lead weight equivalent to 50, 75, and 100% fill fractions. Then expected forces and moments were divided by actual voltage outputs at specific spin and nutation rates to form calibration constants.

At high spin rates ( $\Omega \geq 60$  rpm), the table's structural resonance effectively increased the amplitude of the table motion of the tank location in an unknown way. Therefore, there is no direct way to calibrate the signals. Instead, an indirect semianalytic method was used. To cancel the effect of the unknown table amplitudes, the voltage representing  $M_y$  was divided by the voltage representing  $F_x$  (and similarly for  $M_x/F_y$ ) at each nutation rate. The ratios were normalized by dividing them by the corresponding ratio when the nutation rate equals the spin rate,  $\lambda = \Omega$  at this condition, the tank does not oscillate but merely spins steadily around an axis inclined at  $\theta$  to the vertical, a condition for which



SPIN RATE = 60 RPM  
 FILL FRACTION = 50%  
 TANK DIAMETER = 12 INCHES  
 RADIAL LOCATION = 32 INCHES  
 (CONTROL TANK DATA NOT SHOWN)

Fig. 7 — Typical high spin-speed results

the true moments and forces are easily calculated. From these normalized ratios, along with the known moments and forces at  $\lambda = \Omega$ ; the moment and force data could be calibrated.

### Determining Model Parameters

Slosh resonances were excited in tests driven at low spin rate ( $\Omega \leq 30$  rpm) and high nutation rate ( $\lambda > 80$  rpm). Figure 6 shows a typical result of the oscillating force magnitude. The nutation frequency at which the resonant peak occurs is used to determine the pendulum length  $l_s$ . (Only the lower of the two slosh resonances mentioned in the third section of this report was observed because the second frequency is above the nutation capability of the table.) The height of the resonant peak force above the equivalent rigid-liquid baseline and the width of the resonant curve are sufficient to determine the pendulum mass  $M_s$  and the viscous dashpot  $C_s$  [3].

The magnitude of the rigidly attached mass  $M_0$  equals the difference between the total liquid mass and the pendulum mass ( $M_T - M_s$ ). From considerations of symmetry, both  $M_0$  and the pendulum hinge point must be located at the center of the tank, independently of the fill level [3]. Similar data analyses determine the parameters of the pendulum model for all fill levels, spin rates, and liquid viscosities. The results for  $M_0$ ,  $M_s$ , and  $l_s$  are not markedly different from those found previously for a nonspinning spherical tank [3] with the exception that the viscous damping is three to five times greater for the spinning tank. A nonlinear liquid response at resonance complicated data reduction. The nodal line of the surface wave rotated around the tank. Similar behavior has been observed in nonspinning spherical tanks [3].

Inertial wave resonances, if they exist, should be excited in tests driven at large spin rates ( $\Omega \geq 60$  rpm) and small nutation rates ( $\lambda < 40$  rpm). The data did not, however, reveal any resonances that

were large enough to note in the moment measurements. Because the moments were measured about an axis that did not pass through the center of the tank, the data had to be analytically adjusted to subtract out the large moment of the oscillating liquid force about the dynamometer axis. Even though this type of data reduction has some inherent inaccuracy, there was no evidence of resonances. After correcting the data as indicated, the moment about the tank center, which is due to the viscous shear at the wall, can be determined. Figure 8 shows a typical result. The straight line fitted through the data is the type of correlation expected for an unsteady viscous boundary layer, in which the bulk of the liquid is unperturbed from its state of steady spinning. (The data shown in the plot do not exactly fall on a straight line, even allowing for the rather large scatter; but, the curvature of the data is not always evident in other tests and in some tests displayed the opposite curvature. A straight line relation implies that the viscous shear is linearly dependent on the oscillatory rotation rate of the tank and represents the best correlation for all the data.) This type of moment data is sufficient to determine the magnitude of the viscous dashpot that represents the viscous boundary layer at the wall, The best fit correlation is

$$C = 34.1 \rho d^5 \Omega F_w (v/\Omega d^2)^{1/2} \text{ in-lbf-s,} \quad (2)$$

where,  $0 \leq F_w \leq 1$  is the fraction of the wall wetted by the liquid;  $F_w$  depends on the fill level. The measured viscous shear is several orders of magnitude larger than would be predicted by a laminar flow analysis; this result is in agreement with data presented by Vanyo [6,7]. The energy dissipation rates are also correspondingly larger.

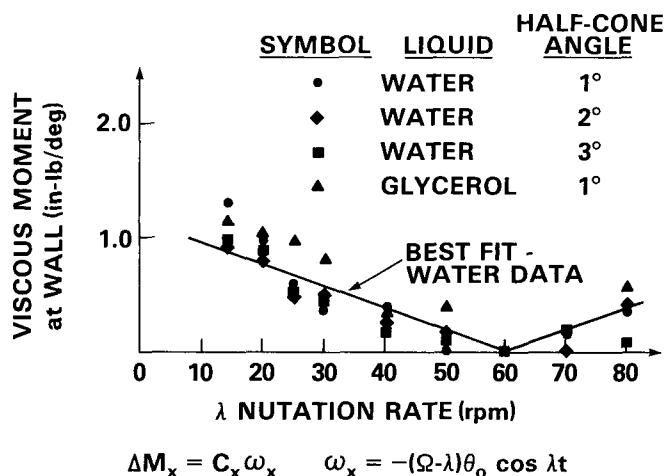


Fig. 8 — Wall shear moment for half-full tank at 60-rpm spin rate

The apparent lack of an inertial wave resonance implies that viscous coupling of the liquid bulk to the oscillatory tank rotation (which is simulated by the dashpot  $C$  in the model) is too weak to cause a noticeable deviation of the liquid from a steady state spin. This observation agrees with previous qualitative tests [8]. The mechanical model also predicts that an inertial wave resonance in a spherical tank would be rather small, regardless of the magnitude of the dashpot constant. That is, the dashpot (liquid viscosity) drives the liquid motion as well as damps it. If the dashpot constant is large, the driving moment on the rotor (that is, the liquid) would be large but so would the damping. Conversely, if the dashpot constant is small, the damping is small but so is the driving moment. Thus the resonance will always be a small effect in comparison to the large resonances driven directly by rotation motion of nonspherical tanks [4].

Not all inertial wave model parameters could have been determined by test data even if an inertial wave resonance had been observed. The resonant peak moment, resonant frequency, and resonant

curve width would only be sufficient to determine certain ratios of model parameters, such as  $I_z/I_x$ ,  $I_z/I_y$ ,  $k_x C_x/D_x$ , and  $k_y C_y/D_y$ . These ratios, however, are all that are needed to compute energy dissipation rates both at the resonant frequency and at nutation rates far removed from resonance. Thus the lack of definiteness would not be a drawback in applications. The uncertainty of the model parameters does point out, nonetheless, the need for a complete theory of liquid motions in a spinning, nutating spherical tank.

## SCALING RELATIONS

One of the advantages of an equivalent mechanical model in interpreting and generalizing laboratory data is that the model itself can be used to predict on-orbit conditions; otherwise, the test data would have to be scaled directly. The way the model parameters depend on spin rate, fill level, viscosity, and other tank and liquid properties can be established more reliably than can the scaling of gross measurements of energy dissipation.

By considering the physical variables that describe liquid motion in a spinning, nutating spherical tank, a set of nondimensional scaling parameters for the model has been formulated by dimensional analysis [9]. Test data were used to determine the importance of the various non-dimensional parameters and to quantify the empirical constants. The scaling relations for the pendulum, or slosh wave, model are:

$$\begin{aligned} &M_0/M_T, \\ &M_s/M_T, \\ &l_s/d, \text{ and} \\ &C_s/M_s l_s^2 \Omega (v^2/d^3 g_{eff})^{0.18}, \end{aligned}$$

where  $g_{eff} = [g^2 + (X_0 \Omega^2)^2]^{1/2}$ . Numerical values of these ratios determined from the tests can be used in the model to compute full-scale, on-orbit energy dissipation rates. For the rotor, or inertial wave model, only the boundary layer dashpot constant was found to be important. This is scaled as follows:

$$C/\rho d^5 \Omega F_w (v/\Omega d^2)^{1/2}.$$

The other parameters of the rotor models should scale as shown:

$$\begin{aligned} &I_z/I_x, \\ &I_z/I_y, \\ &k_x, k_y, \\ &e_x, e_y, \text{ and} \\ &D/\rho d^5 \Omega (v/\Omega d^2)^n. \end{aligned}$$

However, since no inertial wave resonances were found, numerical values of these parameters could not be established.

## SUMMARY

This report describes a laboratory based method to estimate energy dissipation rates for prolate spinning spacecraft. A forced motion drive table was designed and constructed to spin and nutate scale model propellant tanks. Because the nutation frequency can be adjusted independently of the spin rate, the table is able to excite all important liquid resonance frequencies and measure forces and moments throughout the range of interest.

The experimental data were used to determine the parameters of an empirical mechanical model of the liquid motion dynamics. In the model, a pendulum represents the free surface modes of oscillation (sloshing) and a rotor represents the inertial wave modes of oscillation. The rotor is connected to the tank by a dashpot that simulates the forcing of inertial waves by the boundary layer shear at the tank wall. Other dashpots are used to simulate the viscous damping of the slosh and inertial wave modes.

The test results and model determinations have shown that the sloshing modes in a spinning spherical tank are not significantly different from those determined previously for nonspinning tanks, with the exception that the damping is increased by a factor of three to five. The tests also show that no inertial wave mode is excited to a significant amplitude by the boundary layer shear in a spinning, nutating spherical tank. However, the boundary layer effect and the corresponding energy dissipation are much larger than would be anticipated on the basis of a laminar flow analysis.

## ACKNOWLEDGMENTS

We acknowledge the help of other team members who strived to ensure the forced motion stand yielded credible data outputs and who operated under the compromises between desired testing conditions vs realistic hardware limitations. We are indebted to Tom Dilello for constructing electronics cables, circuit filters, multiprogrammer interfaces to the stand's controlling computer, and developing software; Daniel Clark for building the strain gage instrumentation and other electromechanical interfaces; and Russ Barnes and his technical staff who designed, built, and maintained the test hardware.

## REFERENCES

1. F. Pfeiffer, "On Contained Rotating Fluids in Satellite Dynamics," Intelsat/ESA Colloquium on Dynamic Effects of Liquids on Spacecraft Attitude Control, Washington, D.C., April 25-26, 1984.
2. H.P. Greenspan, *The Theory of Rotating Fluids* (Cambridge University Press, 1969).
3. H.N. Abramson, ed. "The Dynamic Behavior of Liquids in Moving Containers," NASA, SP-106, 1966. (Reprinted with corrections by Southwest Research Institute, San Antonio, 1980.)
4. K.D. Aldridge and A. Toomre, "Axisymmetric Inertial Oscillations of a Fluid in a Rotating Spherical Container," *J. Fluid Mech.* **37**(2), 307-323 (1969).
5. K. Stewartson, "On the Stability of a Spinning Top Containing Liquid," *Fluid Mech.* **5**, 577-592 (1959).
6. J.P. Vanyo, "An Energy Assessment for Liquids in a Filled Precessing Spherical Tank," *J. Appl. Mech.* **40** 851-856 (1973).
7. J.P. Vanyo, "Fluid Velocities and Energy Dissipation: Experiments," Intelsat/ESA Colloquium on Dynamic Effects of Liquids on Spacecraft Attitude Control, Washington, D.C., April 25-26, 1984.
8. E. R. Martin, "Experimental Investigations on the Fuel Slosh of Dual-Spin Spacecraft," *COMSAT Technical Review* **1**(1), 1-20 (1971).
9. W. E. Baker, P. S. Westine, and F. T. Dodge, *Similarity Methods in Engineering Dynamics* (Spartan Books, Washington, D.C., 1973).

## Appendix ANALYSIS OF MODELS

### COORDINATE SYSTEMS

Figure A1(a) shows that the equilibrium (nonnutating) position of the tank center is  $X' = X_0$ ,  $Y' = 0$ ,  $Z' = Z_0$ , referred to a rotating  $X'$ ,  $Y'$ ,  $Z'$  system located at the pivot point of the forced motion drive system. The equations of the model are developed in a body fixed set of axes  $x$ ,  $y$ ,  $z$ , which for clarity are referred to an  $X$ ,  $Y$ ,  $Z$  rotating system similar to  $X'$ ,  $Y'$ ,  $Z'$  but located at the tank center. The angular rates about the  $x$ ,  $y$ ,  $z$  axes to the first order in the half-cone angle  $\theta$  are

$$\omega_x = -(\Omega - \lambda)\theta e^{i\lambda t} \quad (\text{A1a})$$

$$\omega_y = -i(\Omega - \lambda)\theta e^{i\lambda t}, \text{ and} \quad (\text{A1b})$$

$$\omega_z = \Omega, \quad (\text{A1c})$$

where only the real parts have physical meaning.

### PENDULUM MODEL

Figure A1(b) shows that the linearized equations of motion of the pendulum are expressed in terms of small angular displacements  $\alpha$  and  $\psi$ . The displacements are referred to the equilibrium position  $\gamma_0$  of the pendulum as determined by the combined action of gravity  $g$  and centripetal acceleration:

$$\tan \gamma_0 = g/[\Omega^2(X_0 + l_s \cos \gamma_0)]. \quad (\text{A2})$$

At equilibrium, the pendulum lies in the  $x$ ,  $z$  plane.

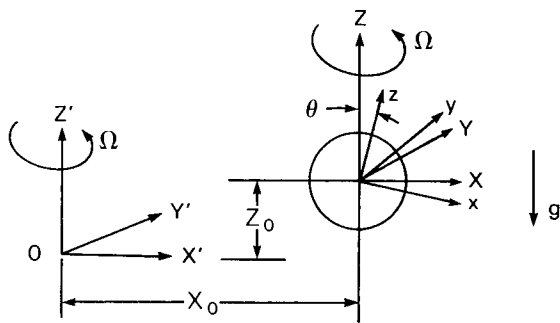


Fig. A1(a) — Coordinate system

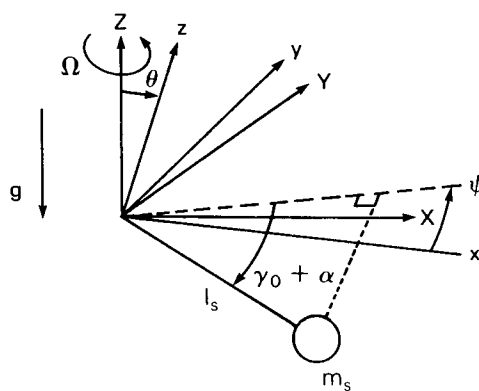


Fig. A1(b) Pendulum model

By considering moments about the hinge point, the equations of motion for  $\alpha$  and  $\psi$  can be shown to be

$$l_s [\ddot{\alpha} + \mu_\alpha^2 \alpha + 2\Omega \dot{\psi} \sin \gamma_0 \cos \gamma_0] = -\theta_0 \sin \gamma_0 [g + (Z_0 - l_s \sin \gamma_0) (\Omega - \lambda)^2] e^{i\lambda t}, \text{ and} \quad (\text{A3a})$$

$$l_s \cos \gamma_0 [\ddot{\psi} + \mu_\psi^2 \psi - 2\Omega \dot{\alpha} \tan \gamma_0] = i\theta_0 [g + (Z_0 - l_s \sin \gamma_0) (\Omega - \lambda)^2] e^{i\lambda t}, \quad (\text{A3b})$$

where

$$\mu_\alpha^2 = \Omega^2 [\cos^2 \gamma_0 + (X_0/l_s \cos \gamma_0)], \text{ and} \quad (\text{A4a})$$

$$\mu_\psi^2 = \Omega^2 (X_0/l_s \cos \gamma_0). \quad (\text{A4b})$$

The effect of damping has been neglected in this derivation, but as customary it can be added later in the resonance terms. Letting  $\alpha_0$  and  $\psi_0$  be the complex steady-state amplitudes of  $\alpha$  and  $\psi$ , the solutions of Eqs. (A3) including damping are

$$\alpha_0 = \theta [(\mu_\psi^2 - \lambda^2) B_0 - 2\Omega \lambda A_0 \sin \gamma_0] / G_0, \text{ and} \quad (\text{A5a})$$

$$\psi_0 = \theta [2\Omega \lambda B_0 \tan \gamma_0 - (\mu_\alpha^2 - \lambda^2) A_0 / \cos \gamma_0] / G_0, \quad (\text{A5b})$$

where

$$A_0 = (g/l_s) + [(Z_0/l_s) - \sin \gamma_0] (\Omega - \lambda)^2, \quad (\text{A6a})$$

$$B_0 = [(X_0/l_s) + \cos \gamma_0] (\lambda^2 - \Omega^2) - A_0 \sin \gamma_0, \text{ and} \quad (\text{A6b})$$

$$G_0 = (\lambda_1^2 - \lambda^2 + 2i\lambda\lambda_1\zeta_{s1}) (\lambda_2^2 - \lambda^2 + 2i\lambda\lambda_2\zeta_{s2}). \quad (\text{A6c})$$

The damping ratios are

$$\zeta_{s1} = C_s / 2M_s l_s^2 \lambda_1, \text{ and} \quad (\text{A7a})$$

$$\zeta_{s2} = C_s / 2M_s l_s^2 \lambda_2, \quad (\text{A7b})$$

and the pendulum natural frequencies are

$$(\lambda_{1,2}/\Omega)^2 = (X_0/l_s \cos \gamma_0) + \frac{1}{2} (1 + 3 \sin^2 \gamma_0)$$

$$\mp [4(X_0/l_s \cos \gamma_0) \sin^2 \gamma_0 + \frac{1}{4} (1 + 3 \sin^2 \gamma_0)^2]^{1/2}. \quad (\text{A8})$$

The  $\lambda_1$  and  $\lambda_2$  cannot be written in terms of an "effective" gravity, say  $[g_0^2 + (X \Omega^2)^2]^{1/2}$ , although the error involved in doing so is not large. In orbit where  $g = 0$ , Eq. (A8) reduces to

$$\lambda_1 = \Omega (X_0/l_s)^{1/2} \text{ and} \quad (\text{A9a})$$

$$\lambda_2 = \Omega [1 + (X_0/l_s)]^{1/2}. \quad (\text{A9b})$$

By comparing these expressions to Eqs. (A4),  $\lambda_1$  is associated with  $\alpha$  resonances (transverse motion) and  $\lambda_2$  is associated with  $\psi$  resonances (circumferential motion).

The components of the liquid force exerted on the tank can be written in terms of  $\alpha$  and  $\psi$ . For example,

$$\begin{aligned} F_x = & -M_T [X_0 + (M_s/M_T) l_s \cos \gamma_0] \Omega^2 - M_T g \theta e^{i\lambda t} \\ & -M_T [Z_0 - (M_s/M_T) l_s \sin \gamma_0] (\Omega - \lambda)^2 \theta e^{i\lambda t} \\ & - \{M_s l_s [(\ddot{\alpha} - \alpha \Omega^2) \sin \gamma_0 + 2\Omega \dot{\psi} \cos \gamma_0]\}. \end{aligned} \quad (\text{A10})$$

The term in braces represents the effect of pendulum motion (sloshing). The other terms are merely the rigid body response of the total liquid mass,  $M_T = M_0 + M_s$ , concentrated at the center of mass of the liquid.

The energy dissipated per nutation cycle of the liquid motion is

$$E_s = \pi \lambda C_s (|\alpha_0|^2 + |\psi_0|^2). \quad (\text{A11})$$

## ROTOR MODEL

The angular momentum of the steadily rotating liquid is  $I_z \Omega$ , where  $I_z$  is the moment of inertia of the liquid about the  $z$  axis. When inertial oscillations are excited, additional angular momentum is created. This additional momentum about the tank center can be expressed as  $I_x \dot{n}_x$  and  $I_y \dot{n}_y$ , where  $\dot{n}_x$  and  $\dot{n}_y$  are momentum averaged angular rates of liquid. (In the linear approximation, the additional momentum about the  $z$  axis is neglected.)  $I_x$  and  $I_y$  may be thought of as moments of inertia, but they do not have any rigid-body-like relation to  $I_z$  and the geometrical shape of the tank. If  $I_x$  and  $I_y$  can be approximated as time independent, the fluid motion can be modeled as a rotor at the center of the tank. The equations of motion for the rotor are:

$$I_x \ddot{n}_x + D_x \dot{n}_x + (I_z - I_y) \Omega \dot{n}_y = T_x \text{ and} \quad (\text{A12a})$$

$$I_y \ddot{n}_y + D_y \dot{n}_y - (I_z - I_x) \Omega \dot{n}_x = T_y, \quad (\text{A12b})$$

where  $T_x, T_y$  are the moments applied to the liquid by the viscous boundary layer at the tank wall, and  $D_x, D_y$  are the  $x, y$  components of the dashpot shown in Fig. 1.

The viscous moments are modeled as

$$T_x = C_x (1 + i) [\omega_x - k_x \dot{n}_x - i e_x (\Omega/\lambda) (\omega_y - k_y \dot{n}_y)] \text{ and} \quad (\text{A13a})$$

$$T_y = C_y (1 + i) [\omega_y - k_y \dot{n}_y + i e_y (\Omega/\lambda) (\omega_x - k_x \dot{n}_x)], \quad (\text{A13b})$$

where  $C_x, C_y$  are the components of the dashpot  $C$ . The term  $(1 + i)$  represents the fact that an oscillating boundary layer has components of shear that are in phase with both the wall velocity and the wall acceleration\*. Since the liquid "free-stream" velocity at the wall may be greater or less than that indicated by the average rotation rates  $\dot{n}_x$  and  $\dot{n}_y$ , empirical factors  $k_x$  and  $k_y$  are introduced. Considering the smallness of the viscous coupling, an inertial mode that involves a lot of liquid motion in the interior would be one that needs only a small velocity at the wall; that is, the magnitude of  $k_x$  and  $k_y$  would be much less than one. The empirical parameters  $e_x$  and  $e_y$  bring in the Ekman like skewing of a rotating boundary layer. In the following development,  $e_x$  and  $e_y$  are set equal to zero for convenience, but this is not a necessity.

The steady-state amplitudes of the oscillating rotation can be found from Eqs. (A12) and then put into Eqs. (A13) to predict the moments exerted on the tank. Assuming that  $|k_x C_x| \ll 1$  and  $|k_y C_y| \ll 1$  (although neither  $C_x$  nor  $C_y$  need be small), the results are:

$$T_x = -C_x (1 + i) (\Omega - \lambda) \theta e^{i\lambda t} \times \left\{ 1 + \left[ \frac{(1 - i)}{H_0} \left( \frac{k_x C_x}{I_x \lambda_n} \right) \left( \frac{\lambda_n}{\lambda} \right) \right] \left[ \left( \frac{C_y}{C_x} \right) \left( \frac{\Omega}{\lambda} \right) \left( \frac{I_z - I_y}{I_y} \right) - 1 \right] \right\}, \quad (\text{A14})$$

and a similar expression for  $T_y$  with the  $x$  and  $y$  subscripts interchanged and  $\theta$  replaced by  $i\theta$ . The symbol  $H_0$  represents the oscillation effect:

\*H. Schlichting, *Boundary Layer Theory* (McGraw-Hill, New York, 1979), 7th ed.

$$H_0 = 1 - \left( \frac{\lambda_n}{\lambda} \right)^2 - 2i \left[ \zeta_x + \zeta_y + \frac{k_x C_x}{2I_x \lambda_n} + \frac{k_y C_y}{2I_y \lambda_n} \right], \text{ where} \quad (\text{A15})$$

$$\zeta_x = D_x / 2I_x \lambda_n, \text{ and} \quad (\text{A16a})$$

$$\zeta_y = D_y / 2I_y \lambda_n \quad (\text{A16b})$$

are the damping ratios of the inertial oscillation mode. The natural frequency of the mode is:

$$\lambda_n / \Omega = \left[ \left( \frac{I_z - I_y}{I_x} \right) \left( \frac{I_z - I_x}{I_y} \right) \right]^{1/2} \text{ and} \quad (\text{A17})$$

$$(I_z / I_x) > 1 \text{ and } (I_z / I_y) > 1 \text{ for stability.}$$

When the nutation frequency is not close to the natural frequency, the effect of the rotor is small and the moment on the wall reduces, for example, to

$$T_x = -C_x (1 + i) (\Omega - \lambda) \theta e^{i\lambda t}. \quad (\text{A18})$$

Equation (A18) simulates the viscous boundary layer shear. At resonance, where  $\lambda = \lambda_n$ , the wall moment works out to be

$$T_x = -C_x (1 + i) (\Omega - \lambda) \theta e^{i\lambda t} \left\{ 1 + \frac{(1 + i)}{2} \left[ \left( \frac{C_y}{C_x} \right) \left( \frac{\Omega}{\lambda_n} \right) \left( \frac{I_z - I_y}{I_x} \right) - 1 \right] K_0 \right\}, \quad (\text{A18a})$$

where

$$K_0 = \frac{(k_x C_x / I_x \lambda_n)}{(\zeta_x + \zeta_y + (k_x C_x / I_x \lambda_n) + (k_y C_y / I_y \lambda_n))}. \quad (\text{A18b})$$

Since  $\zeta_x$ ,  $\zeta_y$ ,  $C_x$ , and  $C_y$  all represent viscous effects, it can be seen from  $K_0$  that the resonance is bounded (and small) whether  $\zeta_x$ ,  $\zeta_y$ ,  $C_x$ , and  $C_y$  all approach zero or all approach infinity. Wall shear is unaffected by the inertial oscillation if  $C_x = C_y$  and  $I_x = I_y$ , since the term multiplying  $K_0$  is zero.

The energy dissipated by the inertial oscillations is

$$E_I = \pi (\Omega - \lambda) \theta [|T_{xr}| + |T_{yi}|] / \lambda, \quad (\text{A19})$$

where  $T_{xr}$  is the real part of the amplitude of  $T_x$  and  $T_{yi}$  is the imaginary part of the amplitude of  $T_y$ .